Hindawi
International Journal of Chemical Engineering
Volume 2021, Article ID 6621373, 10 pages
https://doi.org/10.1155/2021/6621373

Research Article

Structural and Electrochemical Properties of Lanthanum Silicate Apatites $La_{10}Si_{6-x-0.2}Al_xZn_{0.2}O_{27-\delta}$ for Solid Oxide Fuel Cells (SOFCs)

Shammya Afroze,[1] **Hidayatul Qayyimah Hj Hairul Absah**,[2] **Md Sumon Reza**,[1] **Mahendra Rao Somalu**,[3] **Jun-Young Park**,[4] **Saeed Nekoonam**,[5] **Alibek Issakhov**,[6] **and Abul Kalam Azad**[1]

[1]*Faculty of Integrated Technologies, Universiti Brunei Darussalam, Jalan Tungku Link, Gadong, Bandar Seri Begawan, BE 1410, Brunei Darussalam*
[2]*Faculty of Science, Universiti, Brunei Darussalam Jalan Tungku Link, Gadong, BE 1410, Bandar Seri Begawan, Brunei Darussalam*
[3]*Faculty of Science, Universiti Kebangsaan Malaysia, X 43600 Bangi, Selangor, Malaysia*
[4]*Department of Nanoscience and Advanced Materials Engineering, Sejong University, HMC, 209 Neungdong-ro, Gunja-dong, Gwangjin-gu, Seoul 05006, Republic of Korea*
[5]*Department of Renewable Energies and Environment, Faculty of New Sciences and Technologies, University of Tehran, Tehran, Iran*
[6]*Faculty of Mechanics and Mathematics, Department of Mathematical and Computer Modelling, Al-Farabi Kazakh National University, Almaty, Kazakhstan*

Correspondence should be addressed to Saeed Nekoonam; saeednekoonam@gmail.com and Abul Kalam Azad; abul.azad@ubd.edu.bn

Received 25 October 2020; Revised 18 December 2020; Accepted 6 January 2021; Published 19 January 2021

Academic Editor: Mohammad Hossein Ahmadi

An excellent oxide ion conductivity with high oxygen transportation of lanthanum silicate apatite at the solid oxide fuel cell (SOFC) can be achieved through the solid-state reaction method. The doped $La_{10}Si_{6-x-0.2}Al_xZn_{0.2}O_{27-\delta}$ ($x = 0.2$ and 0.4) materials sintered at 1600°C accomplished crystallinity and crystal structure of apatite-type. The structural and electrochemical characterizations of $La_{10}Si_{6-x-0.2}Al_xZn_{0.2}O_{27-\delta}$ ($x = 0.2$ and 0.4) were executed using X-ray diffraction (XRD), scanning electron microscopy (SEM), energy dispersive X-ray spectroscopy (EDX), and electrochemical impedance spectroscopy (EIS) measurements. The total oxide ion conductivities of $La_{10}Si_{6-x-0.2}Al_xZn_{0.2}O_{27-\delta}$ ($x = 0.2$ and 0.4) were measured from low to intermediate operating temperature range (450 to 800°C) using electrochemical impedance spectroscopy. Room temperature XRD patterns of $La_{10}Si_{6-x-0.2}Al_xZn_{0.2}O_{27-\delta}$ ($x = 0.2$ and 0.4) exhibited $La_{10}Si_6O_{27}$ apatite phase with space group $P6_3/m$ as the main phase with the minor appearance of La_2SiO_5 as an impurity phase. The highest total oxide ion conductivity of 3.24×10^{-3} Scm^{-1} and corresponding activation energy of 0.30 eV at 800°C were obtained for $La_{10}Si_{5.6}Al_{0.2}Zn_{0.2}O_{26.7}$ which contains a low concentration of Al^{3+} dopant.

1. Introduction

Solid oxide fuel cells (SOFCs) are now especially popular with everyone for producing renewable or clean energy gadgets for electricity generation [1, 2]. SOFC provides promising features, such as high performance, environmentally clean power generation, and versatile fuel flexibility (hydrogen, hydrocarbons such as methane, or natural gas [3–8]), as a renewable energy system [9]. One of the most extensively used fuels of SOFC is syngas, produced from the

thermochemical conversion of biomass [10–13]. This electrochemical device is made of dense solid oxide electrolyte located between two perforated electrodes [14–18]. Many researchers have developed new electrolytes that provide stability and high oxide ion or proton conductivity at low to moderate operating temperatures (400 to 700°C) [19–23]. SOFC displays beneficial characteristics at these temperatures, such as a wide variety of materials, longer life and reliability, and low cost. Proton-conducting electrolytes are being tried to substitute yttria-stabilized zirconia (YSZ) [24–27]. One of the recent electrolytes with solid oxide ion conductivity relative to other kinds of materials is lanthanum silicate apatite ($La_{10}Si_6O_{27}$) [27–31]. The conductivity of $La_{10}Si_6O_{27}$ offers oxygen transference numbers near unity over a wide oxygen partial pressure range and stable electrochemical performance under various gas feedstocks [32–36]. The key challenges affecting the stability and electrochemical efficiency of lanthanum silicate materials have low sinterability and the formation of secondary La_2SiO_5 phase [37–39].

Studies on various dopants that can improve the oxide ion conductivity and the interstitial oxide ion concentrations of $La_{10}Si_6O_{27}$ have been carried out [40–42]. The study shows that doping cations on the Si-site have increased the overall oxide ion conductivity of $La_{10}Si_6O_{27}$ than doping on the La-site [34]. Previous researches have also demonstrated that cation vacancies or excess oxygen have increased the oxide ion conductivity of the lanthanum silicate materials [35, 40, 41, 43–46]. Thus, a wide range of cations doping on both La- and Si-sites can enhance the oxide ion conductivity of $La_{10}Si_6O_{27}$ [47].

Recently, the single-chamber solid oxide fuel cell (SC-SOFC) over the conventional SOFC has attracted researchers due to its numerous advantages. SC-SOFC can be operated using a mixture of fuel (where hydrocarbon fuel can be used directly) without sealing [48]. Electrolyte with a porous microstructure can be used in single-chamber SOFC where the snugness of gas is not essential. In SC-SOFC, the catalytic activity occurs only between the electrodes, the partial oxidation of fuel occurs at the anode, and the oxygen reduction occurs at the cathode. Therefore, due to the uniform gas composition, the electromotive force is generated only between the two electrodes and enhances the cell performance due to the use of a mixture of air and hydrocarbon fuel. In Figure 1, methane and oxygen are separated by a porous membrane. The electrochemical reaction occurs with oxygen ions by producing carbon monoxide (CO) and hydrogen (H_2) due to the partial oxidation [48, 49].

The gas transportation through the porous electrolyte can be derived mathematically by viscous flow (Π_v) and Knudsen diffusion (Π_k) [50]:

$$\Pi = \Pi_v + \Pi_k = \frac{\varepsilon r^2}{8\eta\tau RTL}\, Pm + \frac{2\varepsilon\tau}{3\tau\theta_k L}\sqrt{\frac{8}{\pi RMT}}, \quad (1)$$

where ε is the porosity, r is the radius of the pore, η is the gas viscosity, τ is the tortuosity factor, R is the gas constant per mole, T is the temperature, L is the thickness of the porous medium, Pm is the mean pressure, M is the molar mass of the gas, and θ_k is the parameter coefficient of "hardness" of the walls.

In recent research, transition metal dopant such as Zn^{2+} has been found in $La_{10}Si_6O_{27}$ and improved the oxide ion conductivity of $La_{10}Si_6O_{27}$ as reported by Setsoafia et al. [40]. Other research has found that Al^{3+} dopant can also enhance the oxide ion conductivity of $La_{10}Si_6O_{27}$ as investigated by Yoshioka [41] and even by Cao and Jiang [36]. Hence, in this work, a series of new and novel doped $La_{10}Si_6O_{27}$ materials were prepared by codoping of Al^{3+} and Zn^{2+} on the Si- site through solid-state reaction which observed the correlation between sintering temperature and electrical properties. Prepared lanthanum apatite can be used in single-chamber SOFC effectively as a porous electrolyte. Noteworthy, low-cost and low-temperature cell fabrication is possible with these porous electrolytes. Thus, the lanthanum apatite structures could be a novel approach to use in a porous SC-SOFC system that consisted of a porous electrolyte, anode, and cathode as lanthanum apatite has high oxide ion conduction over a wide range of partial pressure of oxygen from 1 to 10^{-21} atm which may accelerate oxide ion conduction with low activation energy. The purpose of this study is to inspect the effects of codoping, varying concentrations of Al^{3+} with a constant concentration of Zn^{2+} on the structure to reduce the energy consumption and the oxide ion conductivity of the lanthanum silicate materials in SOFC (450 to 800°C).

2. Experimental

2.1. Sample Preparation. Lanthanum silicate of $La_{10}Si_{6-x-0.2}Al_xZn_{0.2}O_{27-\delta}$ ($x = 0.2$ and 0.4) samples were synthesized as apatite structure through the solid-state synthesis method [18, 51–56]. Initially, a total of 10 g of appropriate amount of La_2O_3, SiO, Al_2O_3, and ZnO powders were ball milled with 200 g of zirconia balls and 150 ml of ethanol at a rational speed of 250 rpm for 24 hours. After ball milling, the mixtures were then dried completely in an oven at 80°C. The powders were ground and then calcined at 1300°C for 10 hours at 5°C/min heating and cooling rates to get rid of the organics. After calcination, 2.5 g of the powders were pressed uniaxially in a mold at a constant pressure of 50 MPa and a hold-up time of 60 seconds. The produced pellets were sintered at 1600°C for 8 hours at 5°C/min heating and cooling rates.

2.2. Characterization. Structural characterizations of $La_{10}Si_{6-x-0.2}Al_xZn_{0.2}O_{27-\delta}$ ($x = 0.2$ and 0.4) were studied using XRD and SEM, weight %, and atomic % of the elements in the $La_{10}Si_{6-x-0.2}Al_xZn_{0.2}O_{27-\delta}$ ($x = 0.2$ and 0.4) compounds which were measured using EDX. Finally, the electrochemical performances of the electrolytes were investigated using EIS.

Room temperature XRD patterns of the electrolytes were obtained using Cu-K$\propto$1 radiation (wavelength, $\lambda = 1.5406$ Å) with a speed of scan of 2 degrees per minute. Microstructures of the electrolytes were obtained on JEOL

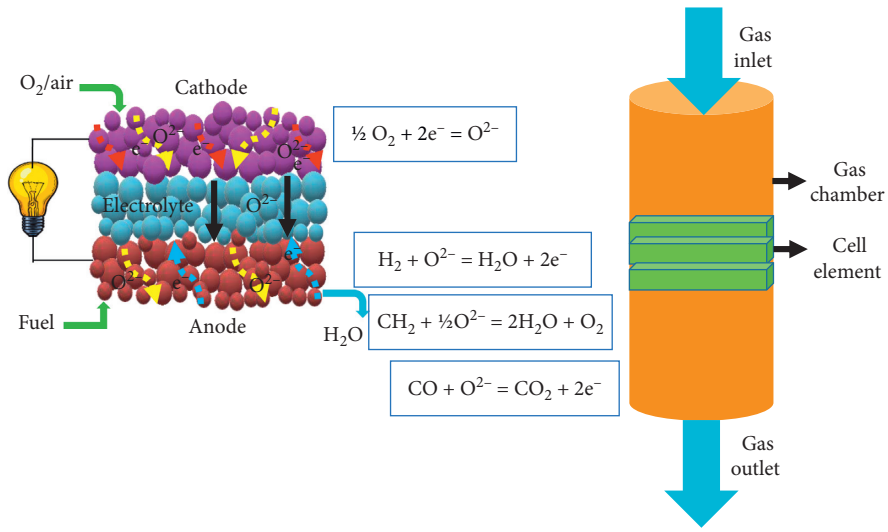

FIGURE 1: Schematic illustration of the all porous single-chamber SOFC. Methane (CH_4) is nourished at the anode side, while air (O_2) is introduced at the cathode and conveyed by the permeable electrolyte to the catalytic anode.

JSM-7610F scanning electron microscopy [57]. EDX is connected to the SEM device to get the weight % and atomic % of the elements in the $La_{10}Si_{6-x-0.2}Al_xZn_{0.2}O_{27-\delta}$ ($x = 0.2$ and 0.4) compounds.

Oxide ion conductivity measurements were performed using a furnace with platinum wires as current collectors. Symmetrical cells with platinum paste coating on the top and bottom surfaces of the pellet were made. A.C. impedance measurements were collected in 50°C steps in the air between 450 and 800°C using a Solartron impedance analyzer system combined with electrochemical interface controlled by Zplot electrochemical impedance software. Total resistance (sum of the bulk and grain boundary resistances) at a certain temperature was obtained from fitting the impedance plot at that temperature. The total oxide ion conductivity σ_{total} was evaluated using the following equation:

$$\sigma_{\text{total}} = \frac{t}{SR}, \tag{2}$$

where t is the thickness of the pellet, S is the surface area of the conducting paste on the pellet, and R is the total resistance. Activation energy was obtained from Arrhenius plot using the following Arrhenius equation:

$$\sigma T = \sigma_o \exp\left(-\frac{E_a}{kT}\right), \tag{3}$$

where σ, σ_o, E_a, k, T are the conductivity (Scm^{-1}), pre-exponential factor, activation energy (eV), Boltzmann constant (8.62×10^{-5} eV/K), and temperature (K), respectively. Equation (3) can be arranged as

$$\log(\sigma T) = -\frac{E_a}{k} \cdot \frac{1}{T} + \log(\sigma_o). \tag{4}$$

3. Results and Discussions

To analyze the apatite structure which was sintered at 1600°C for 8 hours in the air, the X-ray diffraction (XRD) technique was used and represented in Figure 2. The room temperature XRD patterns of the powder samples confirmed that $La_{10}Si_{6-x-0.2}Al_xZn_{0.2}O_{27-\delta}$ ($x = 0.2$ and 0.4) belongs to an apatite phase of composition $La_{10}Si_6O_{27}$ with space group $P6_3/m$. A small percentage of an impurity phase of La_2SiO_5 was detected from XRD data from the appearance of some additional peaks along with the parent apatite phase. The impurity is difficult to remove once formed even if its appearance in the phase assembly was not thermodynamically favoured [39] and this is the kind of adversity that occurs when a material is made in a solid-state method [58]. The La_2SiO_5 impurity occurred when a secondary phase La_2O_3 formed by decarburization reaction during the calcination reacted with silicate apatite in $La_{10}Si_{6-x-0.2}Al_xZn_{0.2}O_{27-\delta}$ ($x = 0.2$ and 0.4) during the sintering process [29]. La_2SiO_5 crystallizes in the monoclinic symmetry in the $P2_1/c$ space group [59]. The impurity phase is less than 5% which has no significant effect on ionic conduction. The lattice parameters of $La_{10}Si_{5.6}Al_{0.2}Zn_{0.2}O_{26.7}$ were found to be $a = b = 9.71$ Å and $c = 7.21$ Å and the lattice parameters of $La_{10}Si_{5.4}Al_{0.4}Zn_{0.2}O_{26.6}$ were found to be $a = b = 9.73$ Å and $c = 7.21$ Å. The materials have almost similar lattice parameters due to their similar chemical composition and symmetry.

SEM is a powerful technique to understand the density, grain boundaries, and phase purity [60]. Figure 3 shows the morphological structure of the lanthanum silicate apatite of $La_{10}Si_{6-x-0.2}Al_xZn_{0.2}O_{27-\delta}$ ($x = 0.2$ and 0.4) porous electrolytes. It shows that the particles of $La_{10}Si_{6-x-0.2}Al_xZn_{0.2}O_{27-\delta}$ are well connected and form open channels in the electrolyte, which allow gas infiltration through the electrolyte. The cross-section SEM analysis of apatite crystals for the abovementioned compositions showed significant dense solid materials and visible grain size with obvious grain boundaries, which accelerates the exchange of ions indicating electrolytes (Figure 3) [61, 62]. Grain sizes for the samples were approximately 1 μm. Nonuniform grains of $La_{10}Si_{6-x-0.2}Al_xZn_{0.2}O_{27-\delta}$ ($x = 0.2$ and 0.4) indicated that

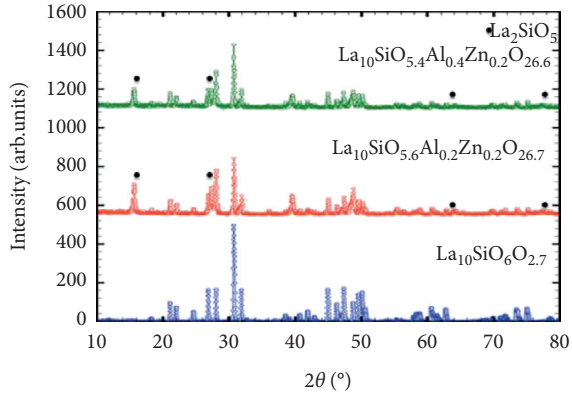

FIGURE 2: Room temperature XRD patterns of $La_{10}Si_{5.6}Al_{0.2}Zn_{0.2}O_{26.7}$ and $La_{10}Si_{5.4}Al_{0.4}Zn_{0.2}O_{26.6}$ sintered at 1600°C for 8 hours in air compared to room temperature XRD pattern of $La_{10}Si_6O_{27}$ sintered at 1500°C for 10 hours in air obtained.

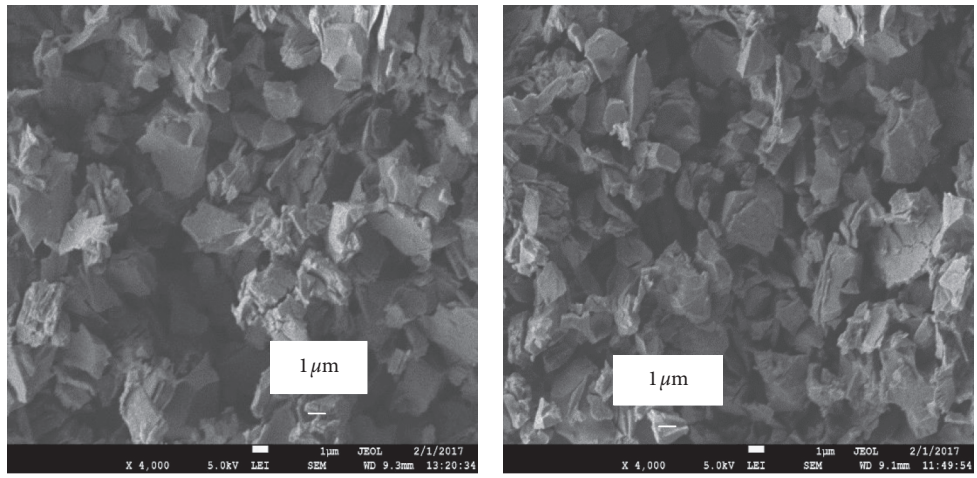

(a) (b)

FIGURE 3: SEM images (cross-sectional) of $La_{10}Si_{5.6}Al_{0.2}Zn_{0.2}O_{26.7}$ (left) and $La_{10}Si_{5.4}Al_{0.4}Zn_{0.2}O_{26.6}$ (right) powders sintered at 1600°C for 8 hours in air.

the milling process had reduced most of the grains into particles of closely related size to each other. This in turn aids in the formation of the apatite structure. Zn and Al codoping at the Si-site increases the density as well as the grain size which increases the ionic conductivity.

At the same time, while running SEM, the energy dispersive X-ray (EDX) analysis was performed with an utterly vacuum atmosphere. The EDX spectra (Figure 4) clearly describes that in addition to a small amount of Al and Zn components, the material contains La, Si, Al, Zn, and O. The particle sizes of $La_{10}Si_{6-x-0.2}Al_xZn_{0.2}O_{27-\delta}$ ($x = 0.2$ and 0.4) were about 1μm. Weight % and atomic % of the sintered powders obtained from EDX spectroscopy are listed in Table 1. Greater weight % of aluminium in $La_{10}Si_{5.4}Al_{0.4}Zn_{0.2}O_{26.6}$ is when the theoretical aluminium content of the $La_{10}Si_{5.4}Al_{0.4}Zn_{0.2}O_{26.6}$ compound is greater than $La_{10}Si_{5.6}Al_{0.2}Zn_{0.2}O_{26.7}$, whereas the weight % of silicon and oxygen are greater in $La_{10}Si_{5.6}Al_{0.2}Zn_{0.2}O_{26.7}$ when the theoretical silicon and oxygen contents of the $La_{10}Si_{5.6}Al_{0.2}Zn_{0.2}O_{26.7}$ compound are greater than the $La_{10}Si_{5.4}Al_{0.4}Zn_{0.2}O_{26.6}$ compound. The weight % of lanthanum and zinc in $La_{10}Si_{6-x-0.2}Al_xZn_{0.2}O_{27-\delta}$ ($x = 0.2$ and 0.4) are closely related values to each other as the theoretical compositions of lanthanum and zinc in $La_{10}Si_{6-x-0.2}Al_xZn_{0.2}O_{27-\delta}$ ($x = 0.2$ and 0.4) compounds are the same. The results show an approximate match between the weight % of elements in a compound and the theoretical composition of the elements in the compound [63].

Figure 5 compares the EIS plots of $La_{10}Si_{6-x-0.2}Al_xZn_{0.2}O_{27-\delta}$ ($x = 0.2$ and 0.4) pellets at 800°C with corresponding equivalent circuit used for fitting the Nyquist plots. The two semicircles of the Nyquist plots represent the grain conductivity and the grain boundary conductivity. The high frequency regime belongs to the grain contribution to the conductivity and the medium range frequency belongs to the grain boundary contribution to the conductivity of $La_{10}Si_{6-x-0.2}Al_xZn_{0.2}O_{27-\delta}$ ($x = 0.2$ and 0.4) [38,64]. The total oxide ion conductivity of $La_{10}Si_{6-x-0.2}Al_xZn_{0.2}O_{27-\delta}$ ($x = 0.2$ and 0.4) at a certain operating temperature was calculated using equation (2) where the total resistance was obtained by fitting

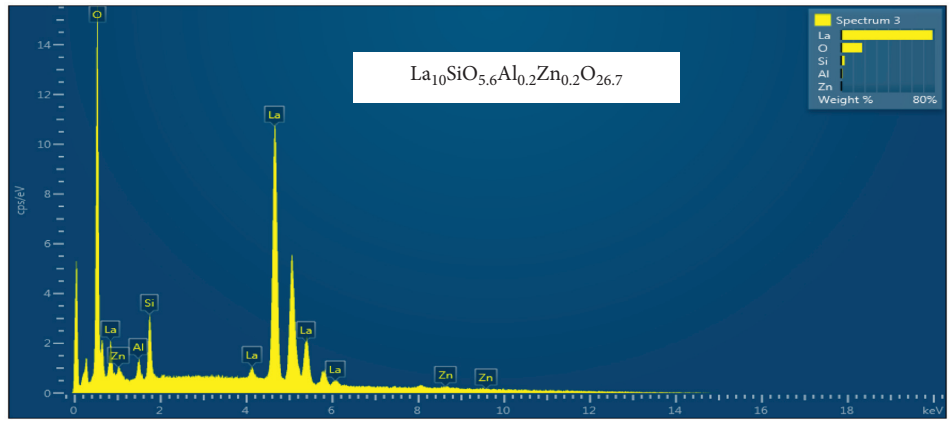

(a)

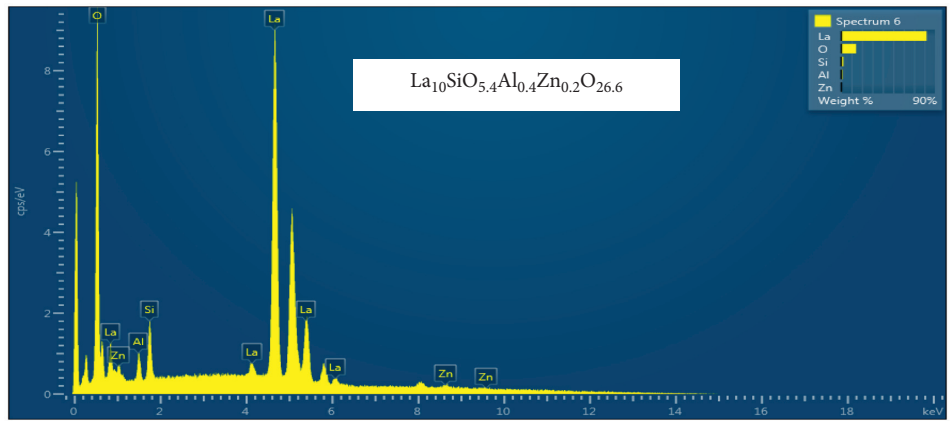

(b)

FIGURE 4: EDX spectra of $La_{10}Si_{5.6}Al_{0.2}Zn_{0.2}O_{26.7}$ (top) and $La_{10}Si_{5.4}Al_{0.4}Zn_{0.2}O_{26.6}$ (bottom) powders sintered at 1600°C for 8 hours in air.

TABLE 1: Elemental distribution of $La_{10}Si_{6-x-0.2}Al_xZn_{0.2}O_{27-\delta}$ ($x = 0.2$ and 0.4) through EDX.

Element symbol	Composition	$x = 0.2$		$x = 0.4$	
		F %	EDX %	F %	EDX %
La	10	77.88	30.73	81.99	36.62
Si	5.6	2.96	5.78	2.16	4.77
Al	0.2	0.98	2	1.17	2.7
Zn	0.2	0.31	0.26	0.35	0.33
O	26.7	17.87	61.24	14.33	55.58

the impedance plot with equivalent circuit model shown as an inset in Figure 5. Total conductivity of different compositions reported in this work and in the literature from 500 to 800°C are listed in Table 2. Overall, it can be stated that the total oxide ion conductivity of $La_{10}Si_{6-x-0.2}Al_xZn_{0.2}O_{27-\delta}$ ($x = 0.2$ and 0.4) pellets gradually increases with increasing temperature as shown in Table 2, which demonstrates that the ionic diffusion process is thermally activated [41]. $La_{10}Si_{5.6}Al_{0.2}Zn_{0.2}O_{26.7}$ obtains the highest total oxide ion conductivity of 3.24×10^{-3} Scm^{-1} at 800°C than $La_{10}Si_{5.4}Al_{0.4}Zn_{0.2}O_{26.6}$ of 2.08 x 10^{-3} Scm^{-1}. The addition of small weight % of aluminium and sintering temperature of 1600°C for 8 hours in air resulted in a good conductivity achieved at the intermediate operating temperature of 800°C. Unfortunately, total oxide ion conductivity measurements of fully sintered $La_{10}Si_{6-x-0.2}Al_xZn_{0.2}O_{27-\delta}$ ($x = 0.2$ and 0.4) pellets could not be obtained because the pellets are not fully sintered even after heating at the maximum temperature (1600°C) of the furnace, whilst the samples have porous electrolyte nature, but the grain growth is obviously aging at elevated temperature which can be correlated with the conductivity results [66]. Normally, Zn doping in oxides increases the sintering behavior and density of the materials [67]. A wet chemical method using azeotropic distillation was used to densify lanthanum silicate. The particle size was about 10 mm which helps to densify the material [68]. Figure 6 presents the Arrhenius plots of $La_{10}Si_{6-x-0.2}Al_xZn_{0.2}O_{27-\delta}$ ($x = 0.2$ and 0.4) pellets. Straight lines can be drawn from the Arrhenius plots that are well fitted to the

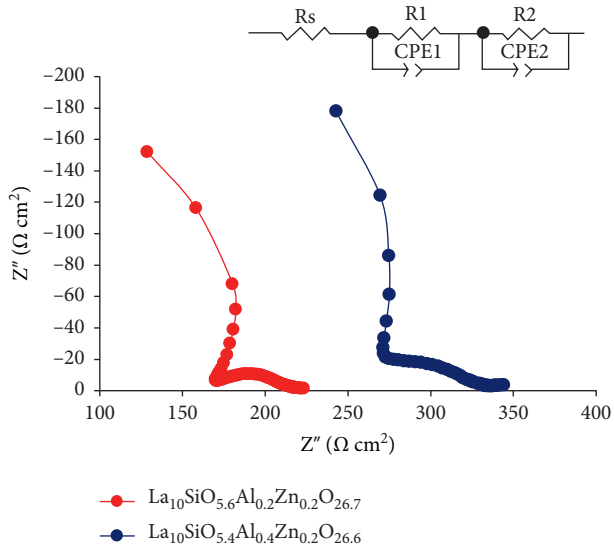

FIGURE 5: A.C. impedance plots of $La_{10}Si_{5.6}Al_{0.2}Zn_{0.2}O_{26.7}$ (left) and $La_{10}Si_{5.4}Al_{0.4}Zn_{0.2}O_{26.6}$ (right) at intermediate operating temperature of 800°C and the equivalent circuit.

TABLE 2: Total conductivity of different compositions reported in this work and in the literature.

Sample compositions	500°C (Scm^{-1})	600°C (Scm^{-1})	700°C (Scm^{-1})	800°C (Scm^{-1})	Ref.
$La_{10}Si_{5.4}Al_{0.4}Zn_{0.2}O_{26.6}$	1.35×10^{-4}	5.67×10^{-4}	1.38×10^{-3}	2.08×10^{-3}	This work
$La_{10}Si_{5.6}Al_{0.2}Zn_{0.2}O_{26.7}$	1.61×10^{-4}	7.23×10^{-4}	1.76×10^{-3}	3.24×10^{-3}	This work
$La_{9.67}Si_6O_{26.5}$	0.40×10^{-3}	—	—	7.10×10^{-3}	[41]
$La_{9.533}(Si_{5.4}Al_{0.6})O_{26}$	0.60×10^{-3}	—	—	7.80×10^{-3}	[41]
$La_{9.8}Si_{5.7}Mg_{0.3}O_{26.4}$	—	—	—	7.40×10^{-2}	[45]
$La_{10}Si_{5.8}Mg_{0.2}O_{26.8}$	—	—	—	8.8×10^{-2}	[45]
$La_9BaSi_6O_{26.5}$	—	—	—	11.4×10^{-3}	[43]
$La_9SrSi_6O_{26.5}$	—	—	—	8.7×10^{-3}	[43]
$La_{9.67}Si_5AlO_{26}$	—	—	—	7.9×10^{-3}	[65]

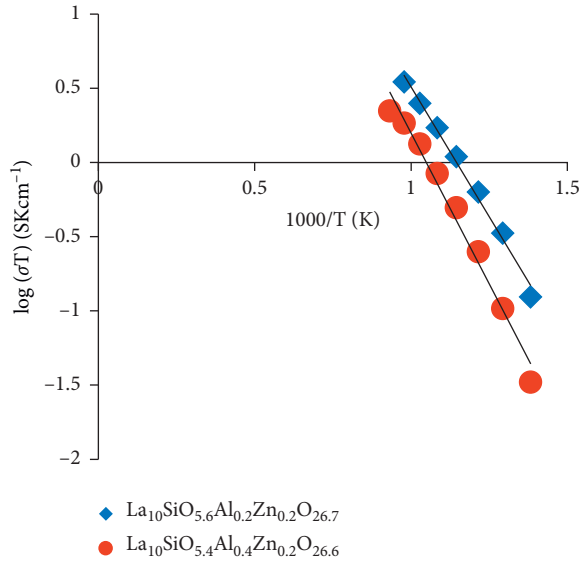

FIGURE 6: Arrhenius plots of total oxide ion conductivity of $La_{10}Si_{6-x-0.2}Al_xZn_{0.2}O_{27-\delta}$ ($x = 0.2$ and 0.4).

Table 3: Comparison of activation energy E_a and preexponential factor k of $La_{10}Si_{6-x-0.2}Al_xZn_{0.2}O_{27-\delta}$ ($x = 0.2$ and 0.4) with literatures.

	$La_{10}Si_{5.4}Al_{0.4}Zn_{0.2}O_{26.6}$ (this work)	$La_{10}Si_{5.6}Al_{0.2}Zn_{0.2}O_{26.7}$ (this work)	$La_{9.6}Si_{5.7}Mg_{0.3}O_{26.1}$ [44]	$La_{10}(SiO_4)_6O_3$ [39]	$La_{10}Si_6O_{27}$ [70]	$La_{9.50}Si_6O_{26.25}$ [70]
Activation energy, E_a (eV)	0.35	0.30	0.43	0.65 ± 0.1	0.67	0.35
Preexponential factor, k ($Skcm^{-1}$)	18281	10216	—	—	—	—

Arrhenius equation. The fitted lines indicate that the diffusion process of oxide ions is thermally activated [45].

The activation energy described by Arrhenius in 1889 is the minimum amount of energy required to conduct a chemical reaction [69], i.e., as less energy is used, the lower the cost. According to the Meyer–Neldel rule, activation energy is related to the preexponential factor, i.e., with the decrease in activation energy, the preexponential factor will increase and the ionic conductivity is affected by temperature significantly compared to the activation energy. From the slope and the intercept of the linear fit in the Arrhenius plots, the activation energy E_a and preexponential factor k of the materials can be obtained using equation (3). The values of activation energy E_a and preexponential factor k of $La_{10}Si_{6-x-0.2}Al_xZn_{0.2}O_{27-\delta}$ ($x = 0.2$ and 0.4) pellets are compared with another apatite structure in Table 3. $La_{10}Si_{6-x-0.2}Al_xZn_{0.2}O_{27-\delta}$ ($x = 0.2$ and 0.4) apatite materials resulted in a significant improvement on the total oxide ion conductivity at the operating temperature of 800°C. It is noteworthy in this work that we got a large value of preexponential factor which may be explicated a higher coordination number between lanthanum (La) and oxygen (O) [71]. Hence, $La_{10}Si_{6-x-0.2}Al_xZn_{0.2}O_{27-\delta}$ ($x = 0.2$ and 0.4) apatite materials maybe useful as electrolyte materials of SOFCs [65]. Recently, lanthanum silicate-based materials were used to measure power density at intermediate temperature [72, 73].

4. Conclusion

In summary, the apatite-type hexagonal $La_{10}Si_{6-x-0.2}Al_xZn_{0.2}O_{27-\delta}$ ($x = 0.2$ and 0.4) crystals were examined as promising electrolytes for SOFCs. Nonetheless, the operational challenges associated with its high sintering temperature. XRD patterns of the sintered $La_{10}Si_{6-x-0.2}Al_xZn_{0.2}O_{27-\delta}$ ($x = 0.2$ and 0.4) materials revealed the apatite phase with $P6_3/m$ space group with a small amount of impurity. The milling process has reduced most of the large grains into microsize grains closely related to each other, which aids in the formation of the hexagonal apatite structure. $La_{10}Si_{5.6}Al_{0.2}Zn_{0.2}O_{26.7}$ gives the highest total oxide ion conductivity of $3.24 \times 10^{-3}\,Scm^{-1}$ at the intermediate operating temperature of 800°C. The activation energy was decreasing with increasing the preexponential factor and the lowest activation energy was 0.30 eV for $La_{10}Si_{5.6}Al_{0.2}Zn_{0.2}O_{26.7}$ which was one of the lowest activation energies among the lanthanum silicate-ion conductors. Thus, the apatite-type $La_{10}Si_{6-x-0.2}Al_xZn_{0.2}O_{27-\delta}$ can be used in SC-SOFCs due to its porous microstructure.

Data Availability

The data used in this study are available on request.

Conflicts of Interest

The authors declare that there are no financial or personal conflicts of interest for this publication.

Acknowledgments

The authors would like to thank the Faculty of Integrated Technologies, Faculty of Science, and Centre for Advanced Material and Energy Sciences at Universiti Brunei Darussalam.

References

[1] M. Beigzadeh, F. Pourfayaz, and M. H. Ahmadi, "Modeling and improvement of solid oxide fuel cell-single effect absorption chiller hybrid system by using nanofluids as heat transporters," *Applied Thermal Engineering*, vol. 166, 2020.

[2] M. Beigzadeh, F. Pourfayaz, M. Ghazvini, and M. H. Ahmadi, "Energy and exergy analyses of solid oxide fuel cell-gas turbine hybrid systems fed by different renewable biofuels: a comparative study," *Journal of Cleaner Production*, vol. 280, 2021.

[3] Z. Wu, P. Zhu, J. Yao et al., "Dynamic modeling and operation strategy of natural gas fueled SOFC-engine hybrid power system with hydrogen addition by metal hydride for vehicle applications," *eTransportation*, vol. 5, 2020.

[4] X. Su, F. Zhang, Y. Yin, B. Tu, and M. Cheng, "Thermodynamic analysis and fuel processing strategies for propane-fueled solid oxide fuel cell," *Energy Conversion and Management*, vol. 204, 2020.

[5] A. M. Abdalla, S. Hossain, O. B. Nisfindy, A. T. Azad, M. Dawood, and A. K. Azad, "Hydrogen production, storage, transportation and key challenges with applications: a review," *Energy Conversion and Management*, vol. 165, pp. 602–627, 2018.

[6] S. Hossain, A. M. Abdalla, S. N. B. Jamain, J. H. Zaini, and A. K. Azad, "A review on proton conducting electrolytes for clean energy and intermediate temperature-solid oxide fuel cells," *Renewable and Sustainable Energy Reviews*, vol. 79, pp. 750–764, 2017.

[7] M. Ahmadi, M. Sadaghiani, F. Pourfayaz et al., "Energy and exergy analyses of a solid oxide fuel cell-gas turbine-organic rankine cycle power plant with liquefied natural gas as heat sink," *Entropy*, vol. 20, no. 7, p. 484, 2018.

[8] M. Beigzadeh, F. Pourfayaz, M. H. Ahmadi, S. M. Pourkiaei, and M. Beigzadeh, "A simplificative approach-based modeling of SOFC power systems fed by natural gas," *Fuel Cells*, vol. 17, no. 6, pp. 843–853, 2017.

[9] N. Mahato, A. Banerjee, A. Gupta, S. Omar, and K. Balani, "Progress in material selection for solid oxide fuel cell technology: a review," *Progress in Materials Science*, vol. 72, pp. 141–337, 2015.

[10] M. S. Reza, A. Ahmed, W. Caesarendra et al., "Acacia holosericea: an invasive species for bio-char, bio-oil, and biogas production," *Bioengineering*, vol. 6, no. 2, p. 33, 2019.

[11] M. S. Reza, S. N. Islam, S. Afroze et al., "Evaluation of the bioenergy potential of invasive *Pennisetum purpureum* through pyrolysis and thermogravimetric analysis," *Energy, Ecology and Environment*, vol. 5, no. 2, pp. 118–133, 2019.

[12] M. S. Reza, C. S. Yun, S. Afroze et al., "Preparation of activated carbon from biomass and its' applications in water and gas purification, a review," *Arab Journal of Basic and Applied Sciences*, vol. 27, no. 1, pp. 208–238, 2020.

[13] M. S. Reza, S. Afroze, M. S. A. Bakar et al., "Biochar characterization of invasive *Pennisetum purpureum* grass: effect of pyrolysis temperature," *Biochar*, vol. 2, no. 2, pp. 239–251, 2020.

[14] J. Hanna, W. Y. Lee, Y. Shi, and A. F. Ghoniem, "Fundamentals of electro- and thermochemistry in the anode of solid-oxide fuel cells with hydrocarbon and syngas fuels," *Progress in Energy and Combustion Science*, vol. 40, no. 1, pp. 74–111, 2014.

[15] S. Afroze, A. Karim, Q. Cheok, S. Eriksson, and A. K. Azad, "Latest development of double perovskite electrode materials for solid oxide fuel cells: a review," *Frontiers in Energy*, vol. 13, no. 4, pp. 770–797, 2019.

[16] H. Q. H. H. Absah, M. S. A. Bakar, J. H. Zaini, A. Azad, and L. C. Ming, "$Bi_2O_3$and $La_{10}Si_6O_{27}$composite electrolyte for enhanced performance in solid oxide fuel cells," *IOP Conference Series: Materials Science and Engineering*, vol. 121, no. 1, 2016.

[17] S. Afroze, M. S. Reza, Q. Cheok, J. Taweekun, and A. K. Azad, "Solid oxide fuel cell (SOFC); A new approach of energy generation during the pandemic COVID-19," *International Journal of Integrated Engineering*, vol. 12, no. 5, pp. 245–256, 2020.

[18] A. K. Azad, A. Kruth, and J. T. S. Irvine, "Influence of atmosphere on redox structure of $BaCe_{0.9}Y_{0.1}O_{2.95}$ - insight from neutron diffraction study," *International Journal of Hydrogen Energy*, vol. 39, no. 24, pp. 12804–12811, 2014.

[19] Z. Zakaria, S. H. Abu Hassan, N. Shaari, A. Z. Yahaya, and Y. Boon Kar, "A review on recent status and challenges of yttria stabilized zirconia modification to lowering the temperature of solid oxide fuel cells operation," *International Journal of Energy Research*, vol. 44, no. 2, pp. 631–650, 2020.

[20] H. Shi, C. Su, R. Ran, J. Cao, and Z. Shao, "Electrolyte materials for intermediate-temperature solid oxide fuel cells," *Progress in Natural Science: Materials International*, vol. 30, no. 6, pp. 764–774, 2020.

[21] A. M. Abdalla, S. Hossain, J. Zhou, P. M. I. Petra, and A. K. Azad, "Synthesis, structural and thermal properties of layered perovskites SmBaMn," *Materials Science Forum*, vol. 889, pp. 195–200, 2017.

[22] S. Hossain, A. M. Abdalla, J. H. Zaini, C. D. Savaniu, J. T. S. Irvine, and A. K. Azad, "Highly dense and novel proton conducting materials for SOFC electrolyte," *International Journal of Hydrogen Energy*, vol. 42, no. 44, pp. 27308–27322, 2017.

[23] A. Afif, J. Zaini, S. M. H. Rahman, S. Eriksson, M. A. Islam, and A. K. Azad, "Scheelite type $Sr_{1-x}Ba_xWO_4$ ($x = 0.1, 0.2, 0.3$) for possible application in solid oxide fuel cell electrolytes," *Scientific Reports*, vol. 9, no. 1, pp. 1–10, 2019.

[24] N. Radenahmad, A. Afif, M. I. Petra, S. M. H. Rahman, S. Eriksson, and A. K. Azad, "High conductivity and high density proton conducting $Ba_{1-x}Sr_xCe_{0.5}Zr_{0.35}Y_{0.1}Sm_{0.05}O_{3-\delta}$ ($x = 0.5, 0.7, 0.9, 1.0$) perovskites for IT-SOFC," *International Journal of Hydrogen Energy*, vol. 41, no. 27, pp. 11832–11841, 2016.

[25] A. Afif, N. Radenahmad, C. M. Lim et al., "Structural study and proton conductivity in $BaCe_{0.7}Zr_{0.25-x}Y_xZn_{0.05}O_3$($x =$ 0.05, 0.1, 0.15, 0.2 & 0.25)," *International Journal of Hydrogen Energy*, vol. 41, no. 27, pp. 11823–11831, 2016.

[26] M. Naeem Khan, A. K. Azad, C. D. Savaniu, P. Hing, and J. T. S. Irvine, "Robust doped $BaCeO_{3-\delta}$ electrolyte for IT-SOFCs," *Ionics (Kiel)*, vol. 23, no. 9, pp. 2387–2396, 2017.

[27] N. Radenahmad, A. Afif, A. M. Abdalla et al., "A new high-performance proton-conducting electrolyte for next-generation solid oxide fuel cells," *Energy Technology*, vol. 8, no. 9, 2020.

[28] S. Nakayama, Y. Higuchi, M. Sugawara, A. Makiya, K. Uematsu, and M. Sakamoto, "Fabrication of c-axis-oriented apatite-type polycrystalline $La_{10}Si_6O_{27}$ ceramic and its anisotropic oxide ionic conductivity," *Ceramics International*, vol. 40, no. 1, pp. 1221–1224, 2014.

[29] W. Liu, S. Yamaguchi, T. Tsuchiya, S. Miyoshi, K. Kobayashi, and W. Pan, "Sol-gel synthesis and ionic conductivity of oxyapatite-type $La_{9.33+x}Si_6O_{26+1.5x}$," *Journal of Power Sources*, vol. 235, pp. 62–66, 2013.

[30] E. Rodríguez-Reyna, A. F. Fuentes, M. MacZka, J. Hanuza, K. Boulahya, and U. Amador, "Facile synthesis, characterization and electrical properties of apatite-type lanthanum germanates," *Solid State Sciences*, vol. 8, no. 2, pp. 168–177, 2006.

[31] J. M. Porras-Vázquez, E. R. Losilla, M. A. G. Aranda, and I. Santacruz, "Oxy-apatite reaction sintering of colloidal and classic ceramic processed powders," *Ceramics International*, vol. 38, no. 3, pp. 1851–1858, 2012.

[32] A. L. Shaula, V. V. Kharton, and F. M. B. Marques, "Oxygen ionic and electronic transport in apatite-type $La_{10-x}(Si,Al)_6O_{26\pm\delta}$," *Journal of Solid State Chemistry*, vol. 178, no. 6, pp. 2050–2061, 2005.

[33] R. Hu, R. Ding, J. Chen, J. Hu, and Y. Zhang, "Preparation and catalytic activities of the novel double perovskite-type oxide La_2CuNiO_6 for methane combustion," *Catalysis Communications*, vol. 21, pp. 38–41, 2012.

[34] D. Marrero-López, M. C. Martín-Sedeño, J. Peña-Martínez et al., "Evaluation of apatite silicates as solid oxide fuel cell electrolytes," *Journal of Power Sources*, vol. 195, no. 9, pp. 2496–2506, 2010.

[35] T. Nakao, A. Mineshige, M. Kobune, T. Yazawa, and H. Yoshioka, "Chemical stability of $La_{10}Si_6O_{27}$ and its application to electrolytes for solid oxide fuel cells," *Solid State Ionics*, vol. 179, no. 27-32, pp. 1567–1569, 2008.

[36] X. G. Cao and S. P. Jiang, "Sinterability and conductivity of barium doped aluminium lanthanum oxyapatite $La_{9.5}Ba_{0.5}Si_{5.5}Al_{0.5}O_{26.5}$ electrolyte of solid oxide fuel cells," *Journal of Alloys and Compounds*, vol. 523, pp. 127–133, 2012.

[37] H. Q. H. H. Absah, A. H. Karim, M. S. Abu Bakar, L. C. Ming, and A. K. Azad, "Synthesis of $La_{10}Si_{6-2x}Bi_{2x}O_{27-x}$ as possible electrolyte materials for solid oxide fuel cells," *Materials Science Forum*, vol. 889, pp. 173–177, 2017.

[38] S. P. Jiang, L. Zhang, H. Q. He, R. K. Yap, and Y. Xiang, "Synthesis and characterization of lanthanum silicate apatite by gel-casting route as electrolytes for solid oxide fuel cells," *Journal of Power Sources*, vol. 189, no. 2, pp. 972–981, 2009.

[39] S. Tao and J. T. S. Irvine, "Preparation and characterisation of apatite-type lanthanum silicates by a sol-gel process," *Materials Research Bulletin*, vol. 36, no. 7-8, pp. 1245–1258, 2001.

[40] D. D. Y. Setsoafia, P. Hing, S. C. Jung, A. K. Azad, and C. M. Lim, "Sol-gel synthesis and characterization of Zn^{2+} and Mg^{2+} doped $La_{10}Si_6O_{27}$ electrolytes for solid oxide fuel cells," *Solid State Sciences*, vol. 48, pp. 163–170, 2015.

[41] H. Yoshioka, "Enhancement of ionic conductivity of apatite-type lanthanum silicates doped with cations," *Journal of the American Ceramic Society*, vol. 90, no. 10, pp. 3099–3105, 2007.

[42] S. Beaudet-Savignat, A. Vincent, S. Lambert, and F. Gervais, "Oxide ion conduction in Ba, Ca and Sr doped apatite-type lanthanum silicates," *Journal of Materials Chemistry*, vol. 17, no. 20, pp. 2078–2087, 2007.

[43] A. Vincent, S. B. Savignat, and F. Gervais, "Elaboration and ionic conduction of apatite-type lanthanum silicates doped with Ba, $La_{10-x}Ba_x(SiO_4)_6O_{3-x/2}$ with x=0.25–2," *Journal of the European Ceramic Society*, vol. 27, no. 2-3, pp. 1187–1192, 2007.

[44] H. Yoshioka and S. Tanase, "Magnesium doped lanthanum silicate with apatite-type structure as an electrolyte for intermediate temperature solid oxide fuel cells," *Solid State Ionics*, vol. 176, no. 31-34, pp. 2395–2398, 2005.

[45] H. Yoshioka, Y. Nojiri, and S. Tanase, "Ionic conductivity and fuel cell properties of apatite-type lanthanum silicates doped with Mg and containing excess oxide ions," *Solid State Ionics*, vol. 179, no. 38, pp. 2165–2169, 2008.

[46] J. E. H. Sansom, E. Kendrick, J. R. Tolchard, M. S. Islam, and P. R. Slater, "A comparison of the effect of rare earth vs. Si site doping on the conductivities of apatite-type rare earth silicates," *Journal of Solid State Electrochemistry*, vol. 10, no. 8, pp. 562–568, 2006.

[47] L. Malavasi, C. A. J. Fisher, and M. S. Islam, "Oxide-ion and proton conducting electrolyte materials for clean energy applications: structural and mechanistic features," *Chemical Society Reviews*, vol. 39, no. 11, pp. 4370–4387, 2010.

[48] M. Kuhn and T. Napporn, "Single-chamber solid oxide fuel cell technology-from its origins to today's state of the art," *Energies*, vol. 3, no. 1, pp. 57–134, 2010.

[49] M. Yano, A. Tomita, M. Sano, and T. Hibino, "Recent advances in single-chamber solid oxide fuel cells: a review," *Solid State Ionics*, vol. 177, no. 39-40, pp. 3351–3359, 2007.

[50] P. P. Mardilovich, Y. She, Y. H. Ma, and M.-H. Rei, "Defect-free palladium membranes on porous stainless-steel support," *AIChE Journal*, vol. 44, no. 2, pp. 310–322, 1998.

[51] S. Afroze, N. Torino, P. F. Henry, M. Sumon Reza, Q. Cheok, and A. K. Azad, "Insight of novel layered perovskite $PrSrMn_2O_{5+\delta}$: a neutron powder diffraction study," *Materials Letters*, vol. 261, 2020.

[52] S. Afroze, N. Torino, P. F. Henry, M. S. Reza, Q. Cheok, and A. K. Azad, "Neutron and X-ray powder diffraction data to determine the structural properties of novel layered perovskite $PrSrMn_2O_{5+\delta}$," *Data in Brief*, vol. 29, 2020.

[53] S. Afroze, N. Torino, M. S. Reza et al., "Structure-conductivity relationship of $PrBaMnMoO_{6-\delta}$ through in-situ measurements: a neutron diffraction study," *Ceramics International*, vol. 47, no. 1, p. 541, 2020.

[54] X. Xu, Y. Xie, S. Ni, A. K. Azad, and T. Cao, "Photocatalytic H_2 production from spinels $ZnGa_2$-CrO_4 ($0 \leq x \leq 2$) solid solutions," *Journal of Solid State Chemistry*, vol. 230, pp. 95–101, 2015.

[55] A. K. M. Zakaria, M. A. Asgar, S.-G. Eriksson et al., "Preparation of Zn substituted Ni-Fe-Cr ferrites and study of the crystal structure by neutron diffraction," *Materials Letters*, vol. 57, no. 26-27, pp. 4243–4250, 2003.

[56] S. Afroze, D. Yilmaz, M. S. Reza et al., "Investigation of structural and thermal evolution in novel layered perovskite $NdSrMn_2O_{5+\delta}$ via neutron powder diffraction and thermogravimetric analysis," *International Journal of Chemical Engineering*, vol. 2020, Article ID 6642187, 7 pages, 2020.

[57] JEOL Ltd, A Guide to Scanning Microscope Observation published by, JEOL Ltd., Akishima, Tokyo, Japan, https://www.jeol.co.jp/en/applications/pdf/sm/844_en.pdf.

[58] Y. Zhao, L. Dai, Z. He, L. Wang, and J. Cao, "Synthesis and characterization of Ba^{2+} and W^{6+} co-doped apatite-type lanthanum silicate electrolytes," *Ceramics International*, vol. 46, no. 4, pp. 5420–5429, 2020.

[59] K. Fukuda, T. Iwata, and E. Champion, "Crystal structure of lanthanum oxyorthosilicate, La_2SiO_5," *Powder Diffraction*, vol. 21, no. 4, pp. 300–303, 2006.

[60] Y. Zhang, Z. Su, A. K. Azad, W. Zhou, and J. T. S. Irvine, "Directly imaging interstitial oxygen in silicate apatite," *Advanced Energy Materials*, vol. 2, no. 3, pp. 316–321, 2012.

[61] T. Yang, H. Zhao, M. Fang, K. Świerczek, J. Wang, and Z. Du, "A new family of Cu-doped lanthanum silicate apatites as electrolyte materials for SOFCs: synthesis, structural and electrical properties," *Journal of the European Ceramic Society*, vol. 39, no. 2-3, pp. 424–431, 2018.

[62] M. Irshad, Q. u. Ain, K. Siraj et al., "Evaluation of $BaZr_{0.8}X_{0.2}$ (X= Y, Gd, Sm) proton conducting electrolytes sintered at low temperature for IT-SOFC synthesized by cost effective combustion method," *Journal of Alloys and Compounds*, vol. 815, p. 152389, 2020.

[63] S. Afroze, A. M. Abdalla, N. Radenahmad, Q. C. Hoon Nam, and A. K. Azad, "Synthesis, structural and thermal properties of double perovskite $NdSrMn_2O_6$ as potential anode materials for solid oxide fuel cells," in *Proceedings of the 7th Brunei International Conference on Engineering and Technology 2018 (BICET 2018)*, vol. 2018, Bandar Seri Begawan, Brunei, November 2018.

[64] I. Yasuda, Y. Matsuzaki, T. Yamakawa, and T. Koyama, "Electrical conductivity and mechanical properties of alumina-dispersed doped lanthanum gallates," *Solid State Ionics*, vol. 135, no. 1-4, pp. 381–388, 2000.

[65] H. Li, S. Zhang, S. Zhou, and X. Cao, "Chemical bond characteristics, thermal expansion property and compressibility of AR_2O_4 (A=Ca, Sr, Ba; R=rare earths)," *Materials Chemistry and Physics*, vol. 114, no. 1, pp. 451–455, 2009.

[66] X. Ding, G. Hua, D. Ding, W. Zhu, and H. Wang, "Enhanced ionic conductivity of apatite-type lanthanum silicate electrolyte for IT-SOFCs through copper doping," *Journal of Power Sources*, vol. 306, pp. 630–635, 2016.

[67] A. Azad and J. Irvine, "High density and low temperature sintered proton conductor $BaCe_{0.5}Zr_{0.35}Sc_{0.1}Zn_{0.05}O_{3-\delta}$," *Solid State Ionics*, vol. 179, no. 19-20, pp. 678–682, 2008.

[68] H.-C. Yao, J.-S. Wang, D.-G. Hu, J.-F. Li, X.-R. Lu, and Z.-J. Li, "New approach to develop dense lanthanum silicate oxyapatite sintered ceramics with high conductivity," *Solid State Ionics*, vol. 181, no. 1-2, pp. 41–47, 2010.

[69] N. S. Khan, Z. Shah, M. Shutaywi, P. Kumam, and P. Thounthong, "A comprehensive study to the assessment of Arrhenius activation energy and binary chemical reaction in swirling flow," *Scientific Reports*, vol. 10, no. 1, p. 7868, 2020.

[70] J. Chen, J. Huang, X. Li et al., "Plasma-sprayed coating of an apatite-type lanthanum silicate electrolyte for intermediate temperature solid oxide fuel cells (IT-SOFCs)," *Plasma Science and Technology*, vol. 15, no. 7, pp. 673–676, 2013.

[71] N. Takeda, Y. Itagaki, and Y. Sadaoka, "Relationship between pre-exponential factor and activation energy of conductivity in sintered $ln_{9.33+x/3}Si_{6-x}M_xO_{26}$ (Ln=La, Nd, Sm, M=Al, Gd) with apatite-like structure," *Journal of the Ceramic Society of Japan*, vol. 115, no. 1346, pp. 643–647, 2007.

[72] A. Mineshige, A. Saito, M. Kobayashi et al., "Lanthanum silicate-based layered electrolyte for intermediate-temperature fuel cell application," *Journal of Power Sources*, vol. 475, p. 228543, 2020.

[73] J. R. Tolchard, J. E. H. Sansom, M. S. Islam, and P. R. Slater, "Structural studies of apatite-type oxide ion conductors doped with cobalt," *Dalton Transactions*, vol. 20, no. 7, pp. 1273–1280, 2005.